Prostate Cancer: Correlation of MR Imaging and MR Spectroscopy with Pathologic Findings after Radiation Therapy—Initial Experience[1]

Darko Pucar, MD, PhD
Amita Shukla-Dave, PhD
Hedvig Hricak, MD, PhD
Chaya S. Moskowitz, PhD
Kentaro Kuroiwa, MD, PhD
Semra Olgac, MD
Lanie E. Ebora, BS
Peter T. Scardino, MD
Jason A. Koutcher, MD, PhD
Kristen L. Zakian, PhD

Published online before print
10.1148/radiol.2362040739
Radiology 2005; 236:545–553

Abbreviations:
Cho = choline
Cit = citrate
Cr = creatine
PSA = prostate-specific antigen
SNR = signal-to-noise ratio

[1] From the Departments of Radiology (D.P., A.S.D., H.H., L.E., J.A.K., K.L.Z.), Medical Physics (D.P., A.S.D., L.E., J.A.K., K.L.Z.), Epidemiology and Biostatistics (C.M.), Urology (K.K., P.T.S.), Pathology (K.K., S.O.), and Medicine (J.A.K.), Memorial Sloan-Kettering Cancer Center, 1275 York Ave, New York, NY 10021. Supported by National Institutes of Health grant R01 CA76423. Received April 23, 2004; revision requested June 3; revision received December 14; accepted December 20. **Address correspondence to** A.S.D. (e-mail: *davea@mskcc.org*).

Authors stated no financial relationship to disclose.

Author contributions:
Guarantor of integrity of entire study, H.H.; study concepts, H.H., D.P., A.S.D.; study design, D.P., A.S.D., H.H.; literature research, D.P., A.S.D.; clinical studies, D.P., A.S.D., H.H., K.K., S.O., L.E., P.T.S., J.A.K., K.L.Z.; data acquisition, D.P., A.S.D., K.K., K.L.Z.; data analysis/interpretation, D.P., A.S.D., H.H., C.M., K.K., S.O., L.E., J.A.K., K.L.Z.; statistical analysis, C.M.; manuscript preparation, D.P., A.S.D., H.H., C.M.; manuscript definition of intellectual content, D.P., A.S.D., H.H., P.T.S.; manuscript editing, D.P., A.S.D., H.H., C.M.; manuscript revision/review and final version approval, all authors

PURPOSE: To prospectively evaluate magnetic resonance (MR) imaging and MR spectroscopy for depiction of local prostate cancer recurrence after external-beam radiation therapy, with step-section pathologic findings as the standard of reference.

MATERIALS AND METHODS: Study received institutional approval, and written informed consent was obtained. Study was compliant with Health Insurance Portability and Accountability Act. Sextant biopsy, digital rectal examination, MR imaging, MR spectroscopy, and salvage radical prostatectomy with step-section pathologic examination were performed in nine patients with increasing prostate-specific antigen levels after external-beam radiation therapy. MR imaging criterion for tumor was a focal nodular region of reduced signal intensity at T2-weighted imaging. MR spectroscopic criteria for tumor were voxels with choline (Cho) plus creatine (Cr) to citrate (Cit) ratio ([Cho + Cr]/Cit) of at least 0.5 or voxels with detectable Cho and no Cit in the peripheral zone. Sensitivity and specificity of sextant biopsy, digital rectal examination, MR imaging, and MR spectroscopy were determined by using a prostate sextant as the unit of analysis. For feature analysis, MR imaging and MR spectroscopic findings were correlated with step-section pathologic findings.

RESULTS: MR imaging and MR spectroscopy showed estimated sensitivities of 68% and 77%, respectively, while sensitivities of biopsy and digital rectal examination were 48% and 16%, respectively. MR spectroscopy appears to be less specific (78%) than the other three tests, each of which had a specificity higher than 90%. MR spectroscopic feature analysis showed that a metabolically altered benign gland could be falsely identified as tumor by using MR spectroscopic criteria; further analysis of MR spectroscopic features did not lead to improved MR spectroscopic criteria for recurrent tumor.

CONCLUSION: In summary, MR imaging and MR spectroscopy may be more sensitive than sextant biopsy and digital rectal examination for sextant localization of cancer recurrence after external-beam radiation therapy.

About 25% of all patients that receive a diagnosis of prostate cancer are treated with external-beam radiation therapy (1). Although this method is considered a definitive (curative) treatment for prostate cancer, the reported 5-year prostate-specific antigen (PSA) relapse rate ranges from 15% for low-risk patients to 67% for high-risk patients (2). After PSA relapse, selected patients with biopsy-proved local recurrence, pretreatment clinical stage of T1–T2, no evidence of metastatic disease, and life expectancy of more than 10 years may be selected for salvage radical prostatectomy (3). Diagnosis of local recurrence with digital rectal examination, transrectal ultrasonography (US), and transrectal US–

TABLE 1
PSA Values for Nine Patients

Patient No.	Nadir PSA Level (ng/mL)	PSA Level at MR Imaging (ng/mL)	ASTRO Criteria Satisfied at MR Imaging	Time from MR to Salvage Radical Prostatectomy (mo)	PSA Level at Salvage Radical Prostatectomy (ng/mL)	PSA Level at Salvage Radical Prostatectomy Divided by PSA Level at MR Imaging (ng/mL)
1	0.1	2.37	No	1	2.37	1.00
2	0.2	11.88	Yes	2	11.88	1.00
3	0.4	1.28	Yes	2	1.32	1.03
4	0.66	3.23	Yes	1	3.23	1.00
5	0.36	1.17	No	4	0.97	0.83
6	0.9	6.02	Yes	2	8.5	1.41
7	0.2	1.61	Yes	6	1.92	1.19
8	0.1	2.75	Yes	6	4.48	1.63
9	1.18	3.06	No	4	2.78	0.91

guided sextant biopsy, however, represents a considerable clinical challenge and may require repeated biopsies (2,4).

In the untreated prostate gland, encouraging results in the local staging of prostate cancer with endorectal MR imaging have been reported (5). Although the use of MR imaging in the detection of local recurrence after external-beam radiation therapy has not been studied systematically, MR imaging is generally presumed to be of limited value because of diffuse reduction in signal intensity at T2-weighted MR imaging after radiation therapy, which is caused by glandular atrophy and fibrosis (6–8). Nevertheless, on T2-weighted MR images, detection of nodules that have low signal intensity compared with the surrounding peripheral zone can signify recurrent cancer (8).

Recent developments in MR technology have enabled a three-dimensional metabolic map of the entire prostate gland to be obtained with subcentimeter resolution by using hydrogen 1 (^{1}H) MR spectroscopy (5,9). MR spectroscopy is performed as an adjunct to endorectal MR imaging to allow simultaneous anatomic and metabolic cancer detection. In the untreated gland, MR spectroscopy allows cancer to be distinguished from normal glandular tissue on the basis of an increased choline (Cho) plus creatine (Cr) to citrate (Cit) ratio ([Cho + Cr]/Cit) (9,10). MR spectroscopy has been effective in improving the accuracy of MR imaging in prostate cancer localization and staging (11–13). MR spectroscopic studies in patients treated with hormone therapy showed profound metabolic changes in both normal and malignant tissue, requiring a modification of criteria for cancer detection (14,15). To our knowledge, there are no reported studies of patients treated with external-beam radiation therapy that correlate MR imaging and MR spectroscopic findings with step-section pathologic findings from salvage radical prostatectomy. Thus, the purpose of this study was to retrospectively evaluate MR imaging and MR spectroscopy for depiction of local prostate cancer recurrence after external-beam radiation therapy by using step-section pathologic findings as the standard of reference.

MATERIALS AND METHODS

Patients

Between August 1999 and October 2003, 11 patients underwent combined endorectal MR imaging and MR spectroscopy (study entry time point) after external-beam radiation therapy and prior to salvage radical prostatectomy. Nine of 11 patients (mean age, 59 years; age range, 54–63 years) were included in our retrospective analysis. Two patients, one who underwent chemohormonal therapy prior to salvage radical prostatectomy and another who underwent MR imaging and MR spectroscopy more than 6 months prior to salvage radical prostatectomy, were excluded from data analysis.

The patients enrolled in this study were a subset of an ongoing National Institutes of Health study on the investigation of the value of MR imaging and MR spectroscopy in prostate cancer. The National Institutes of Health study received the institutional approval of the Committee on Human Research, and written informed consent was obtained from all patients. Our study was compliant with the Health Insurance Portability and Accountability Act. These approvals included the ability to conduct subset analysis. The mean radiation dose was 7680 cGy (range, 6660–8100 cGy), and the mean time between external-beam radiation therapy and MR imaging and MR spectroscopic examination was 55 months (range, 22–86 months). At the time of MR imaging and MR spectroscopy, all patients had increasing PSA levels after radiation treatment nadir, and six of nine satisfied the criteria of The American Society for Radiology and Oncology, or ASTRO, consensus panel for radiation therapy failure (three consecutive PSA increases from the nadir after radiation treatment, regardless of the specific PSA values) (Table 1). The patients were selected for salvage radical prostatectomy on the basis of published guidelines (3): *(a)* biopsy-proved local recurrence; *(b)* pretreatment clinical stage of T1–T2 (T1c, two patients; T2a, one patient; T2b, three patients; and T2c, three patients); *(c)* life expectancy of more than 10 years (age range, 54–63 years); and *(d)* no evidence of metastatic disease (Table 2).

After salvage radical prostatectomy, PSA level was undetectable (<0.1 ng/mL) in seven patients, indicating that these patients most likely had only local recurrence and no metastasis. One patient (patient 2) had a low PSA level of 0.22 ng/mL immediately after salvage radical prostatectomy, which decreased to 0.1 ng/mL 2 months later; this was more likely due to positive surgical margins found at pathologic examination than to occult distant metastasis. Patient 6 had persistently high PSA levels, consistent with metastatic disease.

The mean time between MR imaging and MR spectroscopic examination and salvage radical prostatectomy was 3 months (range, 1–6 months). All patients had only a modest increase in PSA level between MR imaging and MR spectroscopic examination and salvage radical prostatectomy (0.83 to 1.63 times) and were considered suitable for correlation of diagnostic findings with step-section pathologic findings (Table 1).

TABLE 2
Metastasis Evaluation Prior to Salvage Radical Prostatectomy

Patient No.	Regional Lymph Nodes at MR or CT	Bone Scan Results	Imaging Findings of Equivocal Lesions on Bone Scans
1	<10 mm	Negative	NA
2	Negative	Negative	NA
3	<10 mm	Equivocal	Degenerative changes at radiography
4	Negative	Equivocal	Negative MR findings
5	Negative	Equivocal	Negative MR findings
6	<10 mm	Negative	NA
7	Negative	Equivocal	Degenerative changes at CT
8	Negative	NA	NA
9	Negative	Negative	NA

Note.—No patients had clinically important nodes (>10 mm largest diameter) at endorectal MR imaging of the pelvis and/or computed tomography (CT) of the abdomen and pelvis. The absence of metastasis in patients with equivocal bone scans was determined with radiography, CT, or MR imaging of suspected lesions. NA = not applicable; the patient did not undergo the test.

Endorectal MR Imaging and MR Spectroscopy

MR imaging and MR spectroscopic technique.—Combined MR imaging and MR spectroscopic examinations were performed with a 1.5-T imager (Signa Horizon; GE Medical Systems, Milwaukee, Wis) by using a phased-array and endorectal coil, as described previously (9–11). Transverse T1-weighted spin-echo MR images were obtained from the aortic bifurcation to the symphysis pubis with the following parameters: repetition time msec/echo time msec, 700/8; section thickness, 5 mm; intersection gap, 1 mm; field of view, 24 cm; matrix, 256 × 192; and two signals acquired. Thin-section high-spatial-resolution transverse and coronal T2-weighted fast spin-echo MR images of the prostate and seminal vesicles were obtained with the following parameters: 4000/96; echo train length, 16; section thickness, 3 mm; intersection gap, 0 mm; field of view, 14 cm; matrix, 256 × 192; and four signals acquired. Transverse T2-weighted MR images were postprocessed to correct for the reception profile of the endorectal coil.

Software developed at the University of California, San Francisco, was used for three-dimensional ^{1}H MR spectroscopic data acquisition and processing (9,16). MR spectroscopic data were acquired by using point-resolved spatially localized spectroscopy, or PRESS, (17) that was optimized for detection of both Cho and Cit. Band-selective inversions with gradient dephasing, or BASING, pulses were used for water and lipid suppression (16). Data sets were acquired as 16 × 8 × 8 (1024 voxels) or 8 × 8 × 8 (512 voxels) phase-encoded arrays with the following parameters: 1000/130, 6.25-mm resolution in all three dimensions, spectral width of 1250 Hz, 512 points, and acquisition time of 17 minutes. Data processing included 2-Hz lorentzian apodization, four-dimensional Fourier transform, and automated frequency, phase, and baseline correction. Spectral data were zero-filled to 3.1-mm resolution in the superior-inferior dimension, resulting in an effective voxel size of 0.12 cm^3 for data analysis; they were then superimposed over transverse T2-weighted MR images to allow simultaneous metabolic and anatomic evaluation. The superimposition was automatic because the MR spectroscopic data were acquired in the same position and with the same gradients as the MR imaging data. Peak areas for Cho, Cr, and Cit were calculated by means of numeric integration. To provide a noise measure, the noise standard deviation over a frequency range equivalent to the peak integration range but in an area containing only noise was calculated for each peak. The peak areas were then normalized with respect to the noise standard deviation to give an approximate signal-to-noise ratio (SNR).

MR image interpretation.—All MR images were interpreted retrospectively by one radiologist (H.H.) with extensive experience (>15 years) in reading prostate endorectal MR images. The reader was aware that patients had recurrent prostate cancer but was unaware of other clinical or MR spectroscopic data or surgical pathologic findings. The MR images were assessed for reduced signal intensity in the peripheral zone at T2-weighted imaging, and the findings were classified in three categories as follows: *(a)* focal (regional) reduction of signal intensity at T2-weighted MR imaging compared with the surrounding peripheral zone, and the region of signal intensity reduction has a nodular shape; *(b)* focal (regional) reduction of signal intensity at T2-weighted MR imaging compared with the surrounding peripheral zone, and the region of signal intensity reduction does not have a nodular shape; and *(c)* diffuse reduction of signal intensity at T2-weighted MR imaging throughout the peripheral zone. This classification system was derived from published data on MR imaging in patients treated with radiation therapy (6–8).

Investigators in a previous study (8) suggested that focal nodular regions of reduced signal intensity at T2-weighted MR imaging can be used to identify tumor after external-beam radiation therapy, and in our study, only this finding was considered a criterion for tumor. The MR imaging feature analysis was used to correlate the three categories of reduced signal intensity at T2-weighted MR imaging outlined earlier by using step-section pathologic findings as the standard of reference.

MR spectroscopic interpretation.—MR spectroscopy data were interpreted by one spectroscopist (A.S.D.) with 3 years of experience in prostate MR spectroscopy. The MR spectroscopic voxels were considered usable for data analysis if they contained at least 75% of peripheral zone tissue, did not include tissue surrounding urethra and ejaculatory ducts, and were free from substantial water and lipid contamination. The metabolite (Cho, Cr, and Cit) peaks were considered to be present at diagnostic levels if the SNR was above the threshold of 3:1. The usable voxels were classified as follows: *(a)* nondiagnostic voxels, voxels with nondiagnostic levels of metabolites; *(b)* Cit voxels, voxels with diagnostic levels of Cit; and *(c)* Cho voxels, voxels with nondiagnostic levels of Cit and diagnostic levels of Cho. On the basis of published data in untreated and hormone-treated gland (9–12,14, 15,18,19), Cit voxels with a (Cho + Cr)/Cit ratio of 0.5 or more and all Cho voxels were considered suspicious (criteria) for tumor in the peripheral zone. To calculate the (Cho + Cr)/Cit ratio in Cit voxels with nondiagnostic levels of Cho and/or Cr, the levels of these metabolites were assigned a value equivalent to the noise standard deviation. The MR spectroscopic feature analysis allowed correlation of Cit and Cho voxels with step-section pathologic findings.

Pathologic Procedure

Pathologic step sections were obtained for correlation with MR imaging and MR spectroscopic findings. Prostatectomy specimens were stained with India ink (green dye on right, blue dye on left) and fixed in 10% formalin for 36 hours. The distal 5 mm of the apex was amputated and coned. The remainder of the gland was serially sectioned from apex to base to obtain transverse slices at 3–4-mm intervals, and the slices were submitted for paraffin embedding as whole mounts. The seminal vesicles were amputated and submitted separately. After paraffin embedding, microsections were placed on glass slides and stained with hematoxylin-eosin. The microsections were reviewed in consensus by two pathologists (K.K. and S.O., with 2 and 4 years of experience in prostate cancer pathologic examination, respectively). The tumor areas were mapped on each slice with a marker. The volumes (in cubic centimeters) of individual tumor foci were calculated with computerized planimetry by using image analysis and measurement software (Image-Pro Plus 4.0; Media Cybernetics, Silver Spring, Md), as described previously (20). The magnitude of radiation-induced effects in benign gland and cancer was also assessed.

Correlation of MR Imaging and MR Spectroscopic Findings with Pathologic Findings

This correlation was conducted by one author (D.P., who had 2 years of experience in MR imaging, MR spectroscopic, and pathologic correlation), who was not involved in the interpretation of MR imaging, MR spectroscopic, and pathologic data. Transverse T2-weighted MR images with superimposed MR spectroscopic data were matched with transverse pathologic step sections on the basis of the following anatomic landmarks: *(a)* the presence of urinary bladder and seminal vesicle tissue on superior sections; *(b)* the section with the largest diameter and progressive changes in the diameter of the sections; *(c)* the section where the ejaculatory ducts enter the verumontanum; *(d)* the anterior and/or posterior and left and/or right position of the ejaculatory ducts and urethra, and the shape of the urethra; *(e)* the thickness of the peripheral zone and the position of the pseudocapsule; and *(f)* the presence, size, and shape of the transition zone. The precision of matching in the superior-inferior direction was estimated as ±1 transverse section (±3 mm). On the basis of these matches, MR imaging and MR spectroscopic findings were correlated with step-section pathologic findings.

Sextant Biopsy and Digital Rectal Examination

The results of sextant biopsy and digital rectal examination were obtained from available clinical reports (data were collected by L.E.E., who had 2 years of experience in prostate cancer data review). Sextant biopsy was performed at one institution in eight of nine patients, and the information about the tumor presence in each sextant was available. Patient 6 underwent biopsy at a different institution, and tumor presence was reported for each lobe. All patients were followed up with serial digital rectal examination, and the tumor location was specified in each sextant.

Data and Statistical Analysis

Sextant tumor localization.—Sextants were defined in the same way on transverse T2-weighted MR images and pathologic step sections. The base included all sections from the superior margin of the prostate bladder up to, but not including, the section with the largest diameter. The midgland included the sections from the section with the largest diameter to the section where ejaculatory ducts enter the verumontanum. The apex included the remaining inferior sections of the prostate. The left and the right sides of the prostate were separated along the median sagittal plane through the verumontanum. A sextant was considered positive at pathologic examination if it contained at least one tumor focus. Tumors could span more than one sextant and were counted as being present in all applicable sextants. Binary MR imaging, MR spectroscopic, biopsy, and digital rectal examination data were obtained for each sextant to determine whether there was at least one tumor in the sextant.

A sextant was classified as positive at MR imaging if it contained at least one focal nodular region of reduced signal intensity at T2-weighted MR imaging. A sextant was classified as positive at MR spectroscopy if it contained at least one suspicious voxel. By using step-section pathologic findings as the standard of reference, the sensitivity and specificity of all diagnostic tests were estimated by using the sextant as the unit of analysis; the methodologic approach was similar to that described in the literature (21). Joint 95% confidence intervals were based on bootstrap percentile intervals (22,23) that take into account the clustering of the multiple tumors and multiple sextants within each patient.

MR spectroscopic feature analysis.—In MR spectroscopic feature analysis, diagnostic voxels (Cit and Cho voxels) were characterized as benign or cancerous. The median (Cho + Cr)/Cit ratios in benign and cancerous Cit voxels were compared by using a permutation test that takes into account the correlation due to the multiple tumors and voxels per patient. In addition, the MR spectroscopic feature analysis was intended to assess whether Cho voxels occur in benign gland. If Cho voxels were found in the benign gland, the Cho SNRs in benign and cancerous Cho voxels were compared by using a permutation test that again accounted for the correlated data. A receiver operating characteristic (ROC) curve was used, with the voxel as the unit of analysis, to aid in assessing the (Cho + Cr)/Cit ratio cutoff for determining voxels suspicious for tumor.

RESULTS

Pathologic Findings

Table 3 provides a summary of pathologic findings. A total of 15 tumors were observed in nine patients: eight clinically important (volume range, 0.22–3.78 cm^3) and seven not considered clinically important (volume range, 0.001–0.060 cm^3). In a total of 54 sextants, 31 were positive for tumor, and the median number of cancerous sextants per patient was three (range, two to six). Eight clinically important tumors were present in 25 sextants, while seven tumors considered not clinically important independently accounted for an additional six positive sextants. Six of nine patients had extraprostatic disease, and in each case, it originated from clinically important tumors. In this study, the volume threshold for clinically important tumor was reduced (0.22 cm^3) from the published threshold (24) in the untreated gland (0.5 cm^3) because two patients had extraprostatic disease that originated from tumors smaller than 0.5 cm^3. Radiation effects were prominent in patient 1, who had tumor that could not be graded and severe atrophy and fibrosis in the benign gland. All other patients had viable tumors and benign glandular tissue that displayed mild atrophy and fibrosis.

TABLE 3
Summary of Pathologic Findings

Patient No.	Gleason Score	Pathologic Stage	No. of Clinically Important Tumors	No. of Tumors Not Considered Clinically Important	No. of Positive Sextants	Sextant Location of Tumors
1	NG	pT2cN0	0	2	2	Right apex, left apex
2	4 + 3	pT3aN0	1	0	4	Left base, right base, right midgland, right apex
3	4 + 4	pT3aN0	1	0	2	Right midgland, right apex
4	4 + 3	pT2cN0	1	1	3	Right midgland, right apex, left apex
5	4 + 3	pT2cN0	1	1	3	Right midgland, right apex, left apex
6	4 + 4	pT3aN1	1	0	2	Right midgland, right apex
7	4 + 4	pT3aN0	1	3	4	Right midgland, right apex, left midgland, left apex
8	4 + 3	pT3aN0	1	0	5	Right base, right midgland, right apex, left midgland, left apex
9	3 + 4	pT3bN0	1	0	6	All sextants

Note.—NG = nongradeable tumor, due to radiation treatment effects.

TABLE 4
Sextant Tumor Localization with MR Imaging, MR Spectroscopy, Sextant Biopsy, and Digital Rectal Examination

Modality	No. of Patients*	No. of Sextants	Sextant Findings				Sensitivity (%)	Specificity (%)
			True-Positive	False-Positive	True-Negative	False-Negative		
MR imaging	9	54	21	1	22	10	68 (51, 85)	96 (88, 100)
MR spectroscopy	9	54	24	5	18	7	77 (63, 90)	78 (59, 96)
Sextant biopsy	8	48	13	1	18	16	45 (31, 60)	95 (77, 100)
Digital rectal examination	9	54	5	1	22	26	16 (3, 39)	96 (86, 100)

Note.—Numbers in parentheses are 95% confidence intervals.
* Patient 6 was excluded from sextant biopsy analysis, since the biopsy result was reported per lobe.

MR Imaging, Sextant Biopsy, and Digital Rectal Examination

MR imaging, sextant biopsy, and digital rectal examination each had more than 90% specificity for sextant tumor localization; however, MR imaging appears to be more sensitive (68%) than sextant biopsy (45%) and digital rectal examination (16%) (Table 4). MR spectroscopy had higher sensitivity (77%) but lower specificity (78%) than other diagnostic tests. Figure 1 provides a representative example of tumor localization with MR imaging and MR spectroscopy.

On T2-weighted MR images, diffuse signal intensity reduction throughout the peripheral zone and a decreased conspicuity of zonal anatomy was observed in all nine patients (Table 5). A focal nodular region of reduced signal intensity at T2-weighted MR imaging with corresponding tumor present at pathologic examination was found in each patient (Table 5). All eight clinically important tumors and one tumor considered not clinically important were detected at MR imaging (Table 3), accounting for 21 true-positive sextants (Table 4). One sextant was false-positive because the nodule was observed in two sextants at MR imaging, while corresponding clinically unimportant tumor was found in only one sextant at pathologic examination. Three focal nonnodular regions of reduced signal intensity at T2-weighted MR imaging were observed in three patients, with no corresponding tumor present at pathologic examination (Table 5).

Of 10 false-negative sextants, five were missed because nodules at MR imaging were observed in fewer sextants than were corresponding clinically important tumors at pathologic examination; in the other five false-negative sextants, no focal reduction of signal intensity at T2-weighted MR imaging was observed, but clinically unimportant tumors were found at pathologic examination.

MR Spectroscopy

By using MR spectroscopic criteria for suspicious voxels, seven of eight clinically important and three of seven clinically unimportant tumors were detected, accounting for 24 true-positive sextants (Tables 3, 4). However, five benign sextants were false-positive on the basis of the same criteria. Of seven false-negative sextants, three were missed because suspicious voxels were present in fewer sextants than were corresponding clinically important tumors at pathologic examination, while undetected tumors accounted for an additional four false-negative sextants. Since the voxels corresponding to missed tumors were either unusable or had nondiagnostic levels of metabolites, false-negative MR spectroscopic findings could not be addressed by changing the criteria for suspicious voxels. However, the criteria were reexamined to address the false-positive MR spectroscopic findings.

Sixty-three Cit voxels were observed in eight patients, whose prostates displayed mild radiation-induced changes at pathologic examination. Forty-two voxels were in benign gland, and 21 voxels were in cancer (Fig 2a). Only patient 1, who had severe atrophy at pathologic examination, did not have Cit voxels. The median (Cho + Cr)/Cit ratio in benign voxels was 0.29 (range, 0.04–7.10), while the median (Cho + Cr)/Cit ratio in cancerous voxels

was 0.70 (range, 0.40–3.70). Despite this trend toward higher (Cho + Cr)/Cit ratios in cancerous voxels, the difference was not statistically significant (P = .135). Only one of 21 (5%) cancerous voxels had a (Cho + Cr)/Cit ratio below the cutoff criterion of 0.5, but seven of 42 (17%) benign voxels had a (Cho + Cr)/Cit ratio of at least 0.5 (range, 0.5–7.1). A receiver operating characteristic analysis of the voxels shown in Figure 2b indicates that the cutoff ratio of 0.5 is reasonable, because with higher cutoffs the sensitivity substantially decreases, and with lower cutoffs the specificity decreases without substantially increasing the sensitivity.

Of 61 Cho voxels in nine patients, 46 were located in cancerous tumor and 15 in benign gland (Fig 2c). The Cho SNR was not significantly higher in the cancerous voxels (P = .406), with a median Cho SNR in cancerous voxels of 6.1 (range, 3.0–13.6) and a median Cho SNR in benign voxels of 5.1 (range, 3.6–12.1). Although Cho voxels were approximately three times more frequent in cancer than in benign gland, it was not possible to discriminate between individual cancerous and benign Cho voxels with reasonable accuracy.

One hundred thirty-seven nondiagnostic voxels were observed in nine patients. One hundred five were in benign gland, and 32 were in cancer.

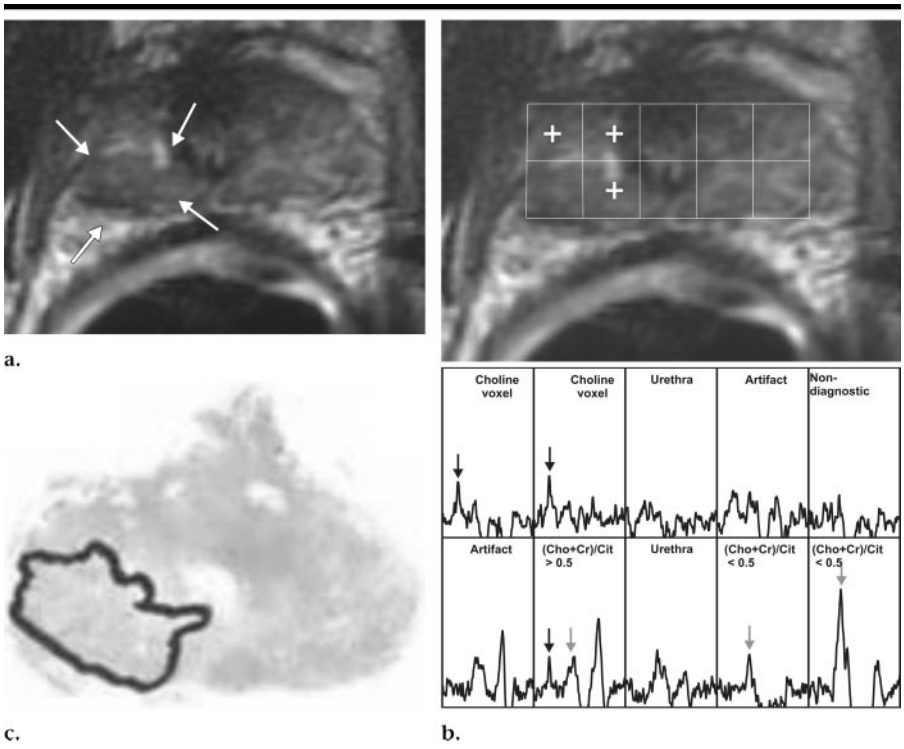

Figure 1. Local prostate cancer recurrence after external-beam radiation therapy, detected with MR imaging and MR spectroscopy. This 63-year-old patient had increasing PSA levels 66 months after completion of external-beam radiation therapy. **(a)** Transverse T2-weighted MR image (4000/96, 14-mm field of view, 3.0-mm section thickness, no intersection gap, 256 × 192 matrix, and four signals acquired) obtained in the prostate apex. A suspicious focal nodular region of reduced signal intensity at T2-weighted MR imaging was observed on the right side (arrows). **(b)** Same transverse T2-weighted MR image with overlaid MR spectroscopic grid; spectra are shown below the image. Spectra were obtained with point-resolved spatially localized spectroscopy, or PRESS, volume excitation with band-selective inversions with gradient dephasing, or BASING, water and lipid suppression (1000/130, 16 × 8 × 8 chemical shift imaging, 100 × 50 × 50-mm field of view, 6.25-mm resolution, one signal acquired, and 17-minute imaging time). Voxels suspicious for cancer are marked with a plus "+" sign. Of three suspicious voxels, two were Cho voxels, while one was a Cit voxel with (Cho + Cr)/Cit ratio of more than 0.5 (Cho and Cit peaks are indicated by black and gray arrows, respectively). Two voxels in benign gland on the left had (Cho + Cr)/Cit ratio of less than 0.5. Two voxels were unusable because of lipid contamination (artifact), while one voxel had no metabolites (nondiagnostic). **(c)** Pathologic slice corresponding to the MR image. The tumor (Gleason score of 4 + 4) was located in the suspicious region at MR imaging and MR spectroscopy.

DISCUSSION

The care of patients with increasing PSA levels after external-beam radiation therapy is difficult from both a diagnostic and a therapeutic standpoint (2,3). Both local and systemic disease are difficult to confirm with available diagnostic methods (2,25). Diagnosis of local recurrence with sextant biopsy is complex because of the uncertainty imposed by sampling error and lack of knowledge of the time required for tumor to become nonviable after radiation therapy (2,4,26). A false-negative rate of 20% was reported at the first biopsy in patients systematically followed up with prostate biopsies after external-beam radiation therapy (4). The interpretation of positive biopsy findings is difficult if the residual tumor shows marked radiation effect and uncertain viability. The only imaging modality with reported diagnostic accuracy for local recurrence after external-beam radiation therapy is transrectal US (49% sensitivity, 57% specificity), which is not superior to digital rectal examination (73% sensitivity, 66% specificity) in the prediction of a positive biopsy result after radiation therapy (27).

Moreover, the sensitivity and specificity of sextant biopsy and transrectal US have not been assessed quantitatively in correlation with step-section pathologic findings, as was done in our study. Radical prostatectomy specimens are the standard of reference for diagnostic tests and the only standard accepted for determination of pathologic tumor stage (28). Salvage radical prostatectomy after external-beam radiation therapy is not commonly performed, however, as the procedure is technically challenging and has higher rates of incontinence, erectile dysfunction, and bladder neck contracture than does primary radical prostatectomy (29,30). Thus, salvage radical prostatectomy is usually reserved only for patients in whom the presence of local recurrence

TABLE 5
Findings of Feature MR Imaging Analysis Correlated with Step-Section Pathologic Findings

Parameter	Focal Nodular	Focal Nonnodular	Diffuse
No. of events	9	3	9
Cancer	9	0	NA
No cancer	0	3	NA

Note.—Columns represent categories of reduced signal intensity at T2-weighted MR imaging. Data are number of events of reduced T2-weighted signal intensity in each category. NA = not applicable.

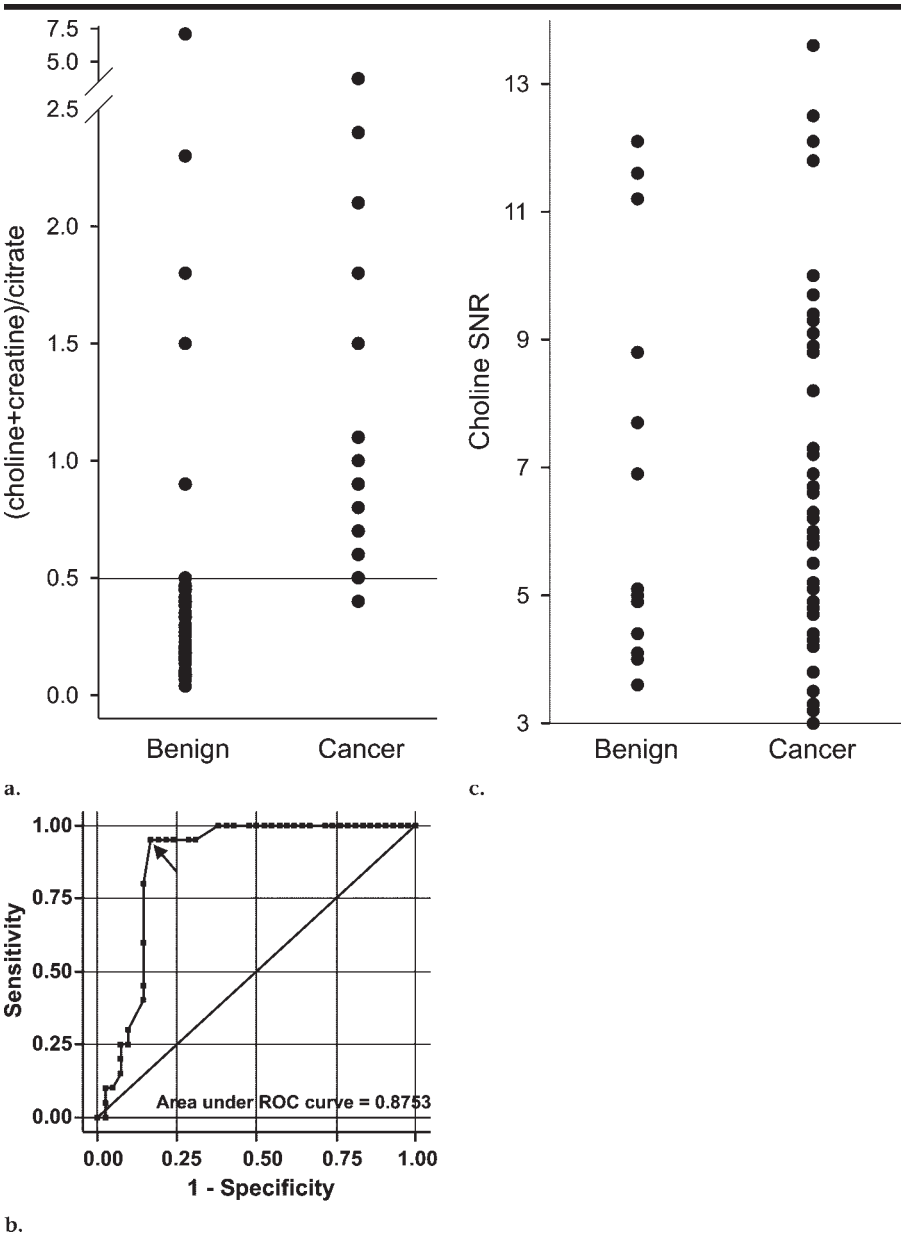

Figure 2. **(a)** The (Cho + Cr)/Cit) ratio in benign and cancerous Cit voxels. Only one of 21 cancerous Cit voxels had (Cho + Cr)/Cit ratio of less than 0.5. **(b)** Receiver operating characteristic curve analysis of (Cho + Cr)/Cit ratio of the voxels shows that the cutoff ratio of 0.5 (arrow) provides a reasonable separation between benign and cancerous Cit voxels in our data set. **(c)** Cho SNR in benign and cancerous Cho voxels. The graph shows Cho SNR overlap between benign and cancerous Cho voxels, precluding their discrimination based on this parameter.

and absence of distant recurrence can be demonstrated conclusively (3,30–32). For that reason, reported series on salvage radical prostatectomy, including ours, have each been based on a small number of highly selected patients (29–32).

The step-section pathologic data provided us with the opportunity to explore MR imaging and MR spectroscopic criteria for cancer detection after external-beam radiation therapy and to assess the accuracy of MR imaging, MR spectroscopy, sextant biopsy, and digital rectal examination for tumor localization by using the sextant as a unit of analysis. When analyzed with our criteria, MR imaging and MR spectroscopy appear to be more sensitive (68% and 77%, respectively) than sextant biopsy and digital rectal examination (48% and 16%, respectively) in sextant tumor localization, suggesting that imaging might be of value in the diagnosis and management of local recurrence. MR imaging and MR spectroscopy could be used to guide biopsy and/or plan treatment. For instance, the knowledge of exact tumor location could help with the decision to preserve or resect the neurovascular bundles at radical prostatectomy (33) or could allow the use of disease-targeting therapies (eg, cryosurgery or high-intensity focused US) (34,35).

The feature analysis suggests that the MR imaging criterion of nodular decrease in signal intensity on T2-weighted images is acceptable for tumor localization. A diffuse reduction in signal intensity on T2-weighted images, described in previous MR imaging studies after radiation therapy (6–8), was found in all patients throughout the peripheral zone, indicating that this change is a consequence of radiation and is unrelated to cancer. During external-beam radiation therapy, the entire prostate is irradiated, leading to diffuse atrophy and fibrosis of glandular tissue (36) that could cause a diffuse reduction in secretion volume and T2-weighted signal intensity. It has been hypothesized that cancer can be detected under such circumstances if it produces an additional focal nodular reduction in signal intensity (8). The results of our study are consistent with this hypothesis, since all focal nodular regions of reduced signal intensity at T2-weighted MR imaging corresponded to tumor pathologic examination.

MR spectroscopic feature analysis showed that benign gland could be identified falsely as cancer with the criteria used in our study. This could be the reason for the apparently lower specificity of MR spectroscopy (78%) in comparison to MR imaging, digital rectal examination, and sextant biopsy, each of which had a specificity of more than 90%. Since previous MR spectroscopic data in patients treated with external-beam radiation therapy were not available, the criteria for tumor were derived on the basis of the studies conducted in untreated and hormone-treated prostate (9–12,14,15,18,19). In the untreated gland, healthy peripheral-zone voxels typically have diagnostic levels of Cit with (Cho + Cr)/Cit ratios less than 0.5 (10), and no Cho voxels are observed (14,15). In contrast, in cancer, the (Cho + Cr)/Cit ratio is increased, and the overlap between the (Cho + Cr)/Cit ratios of benign and cancerous Cit voxels is minimal (10). In addition, only Cho voxels are found in cancer (14,15). In our study, although 17% of benign voxels had (Cho + Cr)/Cit ratios of at least 0.5 after external-beam radiation therapy, receiver operating characteristic analysis indicated that a cutoff (Cho + Cr)/Cit

ratio equal to 0.5 is reasonable and does not need to be increased. In addition, no difference in Cho SNR was found between benign and cancerous Cho voxels. However, Cho voxels and Cit voxels with (Cho + Cr)/Cit ratio of at least 0.5 were around three times more frequent in cancer than in benign gland after external-beam radiation therapy. The current MR spectroscopic criteria (used in our study) may be used to search for local recurrence after external-beam radiation therapy, but the results should be interpreted with caution and correlated with findings of other diagnostic tests.

Our study was not the first to report metabolic alterations after external-beam radiation therapy. When biopsy specimens obtained after external-beam radiation therapy were studied with high-resolution MR spectroscopy, Cit was undetectable in almost all benign and malignant biopsy specimens (37). The exact biochemical mechanisms responsible for these "cancer-like" metabolic alterations in benign gland after radiation or hormone treatment are unknown. A recent study also showed Cit voxels with increased (Cho + Cr)/Cit ratios and Cho voxels in regions with pathologically proved prostatitis in untreated patients (18). Thus, a decrease in Cit and/or an increase in Cho could be a common response to various forms of stress in the prostate (eg, cancer, inflammation, androgen deprivation, and radiation). For instance, it is hypothesized that malignant transformation increases the demand for energy in the prostate, which in turn promotes conversion from Cit-producing to Cit-oxidizing metabolism (38,39). The increased demand for energy could in part be imposed by cellular growth, proliferation, damage, and death, the processes that may increase levels of metabolites, such as Cho, involved in membrane synthesis and degradation (5,40). However, increased energy metabolism and cellular turnover are likely to be present in other stress conditions, as well. The protective effects of stress-induced alterations in energy metabolism were demonstrated in some tissues (41,42). Since eight of nine patients in the present study had viable and metabolically active glands, it is evident that the prostate can withstand and/or recover from radiation injury.

Our study had a number of limitations. The most important limitation was the small sample size, and the results obtained in our exploratory analysis need to be validated prospectively. For instance, the reported sensitivity and specificity of diagnostic tests were only the initial estimates, and a rigorous comparison of the different tests would have to be demonstrated statistically in a larger study to be confirmed. It is possible that a larger study would uncover some weaknesses in apparently adequate MR imaging criteria; conversely, it might produce more refined MR spectroscopic criteria that would be more specific for cancer. Another limitation due to the small sample size was the inability to assess the added value of combined MR imaging and MR spectroscopic readings. On the basis of our data, however, concordant suspicious MR imaging and MR spectroscopic findings (the nodular region of reduced signal intensity at T2-weighted MR imaging displaying abnormal metabolism) strongly suggested cancer, and the optimal interpretation strategy in the presence of discordant MR imaging and MR spectroscopic findings remains to be defined.

Certain limitations were imposed by the MR imaging and MR spectroscopic technology used. MR imaging was performed with standard sequences and without a contrast agent. It is possible that developing further MR imaging methods (eg, use of dynamic contrast material–enhanced or diffusion imaging) would improve cancer detection and/or localization (43–45). MR spectroscopy has a low spectral resolution at 1.5 T that could be improved at higher field strengths. It has recently been reported that at 4 T, it was possible to observe Cho resonance in benign breast tissue that was not visible at 1.5 T (46). The quantification of metabolite levels was relative to noise or to other metabolites, since absolute quantification (concentration determination) has not yet been perfected for the MR spectroscopic method used in our study. Metabolite SNR depends on factors that could vary between voxels in the same patient or between patients (eg, the distance of the voxels from the endorectal coil, the magnetic field homogeneity, and the T1 relaxation times). These factors could have introduced additional variability in our data and impeded the discrimination between benign gland and cancer. The assessment for cancer was performed by using only three metabolites. Additional metabolites (eg, polyamines), detected in the prostate by using high-resolution one- and two-dimensional spectroscopy ex vivo and single-voxel J-resolved spectroscopy in vivo, could eventually be used to improve the diagnostic accuracy of MR spectroscopy (37,47–49).

In summary, our data suggest that MR imaging and MR spectroscopy may be more sensitive than sextant biopsy and digital rectal examination for sextant localization of cancer recurrence after external-beam radiation therapy. The MR imaging criterion for tumor—focal nodular region of reduced signal intensity at T2-weighted MR imaging—was found to be satisfactory in the feature analysis. The MR spectroscopic criteria—Cit voxels with (Cho + Cr)/Cit ratios of 0.5 or more and all Cho voxels—were sensitive for tumor but led to false identification of metabolically altered benign gland as tumor. In our small sample, it was not possible to determine how MR spectroscopic criteria could be improved. Our initial results suggest that it might be beneficial to incorporate MR imaging and MR spectroscopy in the evaluation of patients with increasing PSA levels after external-beam radiation therapy.

References

1. Mettlin CJ, Murphy GP, McDonald CJ, Menck HR. The National Cancer Data Base Report on increased use of brachytherapy for the treatment of patients with prostate carcinoma in the U.S. Cancer 1999; 86: 1877–1882.
2. D'Amico AV, Crook J, Beard CJ, DeWeese TL, Hurwitz M, Kaplan I. Radiation therapy for prostate cancer. In: Walsh PC, Retik AB, eds. Campbell's urology. 8th ed. Philadelphia, Pa: Saunders, 2002; 3147–3170.
3. Scherr D, Swindle PW, Scardino PT. National Comprehensive Cancer Network guidelines for the management of prostate cancer. Urology 2003; 61:14–24.
4. Crook J, Malone S, Perry G, Bahadur Y, Robertson S, Abdolell M. Postradiotherapy prostate biopsies: what do they really mean? results for 498 patients. Int J Radiat Oncol Biol Phys 2000; 48:355–367.
5. Kurhanewicz J, Vigneron DB, Males RG, Swanson MG, Yu KK, Hricak H. The prostate: MR imaging and spectroscopy—present and future. Radiol Clin North Am 2000; 38:115–138.
6. Sugimura K, Carrington BM, Quivey JM, Hricak H. Postirradiation changes in the pelvis: assessment with MR imaging. Radiology 1990; 175:805–813.
7. Coakley FV, Hricak H, Wefer AE, Speight JL, Kurhanewicz J, Roach M. Brachytherapy for prostate cancer: endorectal MR imaging of local treatment-related changes. Radiology 2001; 219:817–821.
8. Nudell DM, Wefer AE, Hricak H, Carroll PR. Imaging for recurrent prostate cancer. Radiol Clin North Am 2000; 38:213–229.
9. Kurhanewicz J, Vigneron DB, Hricak H, Narayan P, Carroll P, Nelson SJ. Three-dimensional H-1 MR spectroscopic imaging of the in situ human prostate with high (0.24-0.7-cm^3) spatial resolution. Radiology 1996; 198:795–805.
10. Males R, Vigneron D, Star-Lack J, et al. Clinical application of BASING and spectral/spatial water and lipid suppression pulses for prostate cancer staging and lo-

calization by in vivo 3D 1H magnetic resonance spectroscopic imaging. Magn Reson Med 2000; 43:17–22.
11. Scheidler J, Hricak H, Vigneron DB, et al. Prostate cancer: localization with three-dimensional proton MR spectroscopic imaging—clinicopathologic study. Radiology 1999; 213:473–480.
12. Wefer AE, Hricak H, Vigneron DB, et al. Sextant localization of prostate cancer: comparison of sextant biopsy, magnetic resonance imaging and magnetic resonance spectroscopic imaging with step section histology. J Urol 2000; 164:400–404.
13. Yu KK, Scheidler J, Hricak H, et al. Prostate cancer: prediction of extracapsular extension with endorectal MR imaging and three-dimensional proton MR spectroscopic imaging. Radiology 1999; 213:481–488.
14. Mueller-Lisse UG, Swanson MG, Vigneron DB, et al. Time-dependent effects of hormone-deprivation therapy on prostate metabolism as detected by combined magnetic resonance imaging and 3D magnetic resonance spectroscopic imaging. Magn Reson Med 2001; 46:49–57.
15. Mueller-Lisse UG, Vigneron DB, Hricak H, et al. Localized prostate cancer: effect of hormone deprivation therapy measured by using combined three-dimensional 1H MR spectroscopy and MR imaging: clinicopathologic case-controlled study. Radiology 2001; 221:380–390.
16. Star-Lack J, Nelson SJ, Kurhanewicz J, Huang LR, Vigneron DB. Improved water and lipid suppression for 3D PRESS CSI using RF band selective inversion with gradient dephasing (BASING). Magn Reson Med 1997; 38:311–321.
17. Bottomley P. Selective volume method for performing localized NMR spectroscopy. US patent 4480228, 1984.
18. Shukla-Dave A, Hricak H, Eberhardt SC, et al. Chronic prostatitis: MRI and 1H MR spectroscopic imaging findings—initial observations. Radiology 2004; 231:717–724.
19. Zakian KL, Eberhardt S, Hricak H, et al. Transition zone prostate cancer: metabolic characteristics at 1H MR spectroscopic imaging—initial results. Radiology 2003; 229:241–247.
20. Villers A, McNeal JE, Freiha FS, Stamey TA. Multiple cancers in the prostate: morphologic features of clinically recognized versus incidental tumors. Cancer 1992; 70: 2313–2318.
21. Obuchowski NA, Lieber ML, Powell KA. Data analysis for detection and localization of multiple abnormalities with application to mammography. Acad Radiol 2000; 7:516–525.
22. Efron B, Tibshirani R. An introduction to the bootstrap. New York, NY: Chapman & Hall, 1993.
23. Pepe M. The statistical evaluation of medical tests for classification and prediction. New York, NY: Oxford University Press, 2003.
24. Bostwick DG, Graham SD Jr, Napalkov P, et al. Staging of early prostate cancer: a proposed tumor volume-based prognostic index. Urology 1993; 41:403–411.
25. Hricak H, Schoder H, Pucar D, et al. Advances in imaging in the postoperative patient with a rising prostate-specific antigen level. Semin Oncol 2003; 30:616–634.
26. Cheng L, Cheville JC, Bostwick DG. Diagnosis of prostate cancer in needle biopsies after radiation therapy. Am J Surg Pathol 1999; 23:1173–1183.
27. Crook J, Robertson S, Collin G, Zaleski V, Esche B. Clinical relevance of trans-rectal ultrasound, biopsy, and serum prostate-specific antigen following external-beam radiotherapy for carcinoma of the prostate. Int J Radiat Oncol Biol Phys 1993; 27:31–37.
28. AJCC cancer staging handbook. 6th ed. Greene FL, Page DL, Fleming ID, et al, eds. New York, NY: Springer-Verlag, 2002; 340–341.
29. Pontes JE, Montie J, Klein E, Huben R. Salvage surgery for radiation failure in prostate cancer. Cancer 1993; 71:976–980.
30. Rogers E, Ohori M, Kassabian VS, Wheeler TM, Scardino PT. Salvage radical prostatectomy: outcome measured by serum prostate specific antigen levels. J Urol 1995; 153:104–110.
31. Gheiler EL, Tefilli MV, Tiguert R, et al. Predictors for maximal outcome in patients undergoing salvage surgery for radio-recurrent prostate cancer. Urology 1998; 51:789–795.
32. Lerner SE, Blute ML, Zincke H. Critical evaluation of salvage surgery for radio-recurrent/resistant prostate cancer. J Urol 1995; 154:1103–1109.
33. Hricak H, Wang L, Wei DC, et al. The role of preoperative endorectal magnetic resonance imaging in the decision regarding whether to preserve or resect neurovascular bundles during radical retropubic prostatectomy. Cancer 2004; 100:2655–2663.
34. Parivar F, Hricak H, Shinohara K, et al. Detection of locally recurrent prostate cancer after cryosurgery: evaluation by transrectal ultrasound, magnetic resonance imaging, and three-dimensional proton magnetic resonance spectroscopy. Urology 1996; 48:594–599.
35. Gelet A, Chapelon JY, Bouvier R, Rouviere O, Lyonnet D, Dubernard JM. Transrectal high intensity focused ultrasound for the treatment of localized prostate cancer: factors influencing the outcome. Eur Urol 2001; 40:124–129.
36. Bostwick DG, Egbert BM, Fajardo LF. Radiation injury of the normal and neoplastic prostate. Am J Surg Pathol 1982; 6:541–551.
37. Menard C, Smith IC, Somorjai RL, et al. Magnetic resonance spectroscopy of the malignant prostate gland after radiotherapy: a histopathologic study of diagnostic validity. Int J Radiat Oncol Biol Phys 2001; 50:317–323.
38. Costello LC, Franklin RB. Bioenergetic theory of prostate malignancy. Prostate 1994; 25:162–166.
39. Costello LC, Franklin RB. Citrate metabolism of normal and malignant prostate epithelial cells. Urology 1997; 50:3–12.
40. Podo F. Tumour phospholipid metabolism. NMR Biomed 1999; 12:413–439.
41. Serafin A, Fernandez-Zabalegui L, Prats N, Wu ZY, Rosello-Catafau J, Peralta C. Ischemic preconditioning: tolerance to hepatic ischemia-reperfusion injury. Histol Histopathol 2004; 19:281–289.
42. Pucar D, Dzeja PP, Bast P, Juranic N, Macura S, Terzic A. Cellular energetics in the preconditioned state: protective role for phosphotransfer reactions captured by 18O-assisted 31P NMR. J Biol Chem 2001; 276:44812–44819.
43. Engelbrecht MR, Huisman HJ, Laheij RJ, et al. Discrimination of prostate cancer from normal peripheral zone and central gland tissue by using dynamic contrast-enhanced MR imaging. Radiology 2003; 229: 248–254.
44. Jennings D, Hatton BN, Guo J, et al. Early response of prostate carcinoma xenografts to docetaxel chemotherapy monitored with diffusion MRI. Neoplasia 2002; 4:255–262.
45. Ogura K, Maekawa S, Okubo K, et al. Dynamic endorectal magnetic resonance imaging for local staging and detection of neurovascular bundle involvement of prostate cancer: correlation with histopathologic results. Urology 2001; 57:721–726.
46. Bolan PJ, Meisamy S, Baker EH, et al. In vivo quantification of choline compounds in the breast with 1H MR spectroscopy. Magn Reson Med 2003; 50:1134–1143.
47. van der Graaf M, Schipper RG, Oosterhof GO, Schalken JA, Verhofstad AA, Heerschap A. Proton MR spectroscopy of prostatic tissue focused on the detection of spermine, a possible biomarker of malignant behavior in prostate cancer. MAGMA 2000; 10:153–159.
48. Swanson MG, Vigneron DB, Tran TK, Sailasuta N, Hurd RE, Kurhanewicz J. Single-voxel oversampled J-resolved spectroscopy of in vivo human prostate tissue. Magn Reson Med 2001; 45:973–980.
49. Swanson MG, Vigneron DB, Tabatabai ZL, et al. Proton HR-MAS spectroscopy and quantitative pathologic analysis of MRI/3D-MRSI-targeted postsurgical prostate tissues. Magn Reson Med 2003; 50:944–954.